Impacts of Burnishing Variables on the Quality Indicators in a Single Diamond Burnishing Operation

Minh-Thai Le[1] – An-Le Van[2,*] – Trung-Thanh Nguyen[3]

[1]Le Quy Don Technical University, Faculty of Special Equipment, Vietnam
[2]Nguyen Tat Thanh University, Faculty of Engineering and Technology, Vietnam
[3]Le Quy Don Technical University, Faculty of Mechanical Engineering, Vietnam

Diamond burnishing is an effective solution to finish a surface. The purpose of the current work is to optimize parameter inputs, including the spindle speed (S), depth of penetration (D), feed rate (f), and diameter of tool-tip (DT) for improving the Vickers hardness (VH) and decreasing the average roughness (Ra) of a new diamond burnishing process. A set of burnishing experiments is executed under a new cooling lubrication system comprising the minimum quantity lubrication and double vortex tubes. The Bayesian regularized feed-forward neural network (BRFFNN) models of the performances are proposed in terms of the inputs. The criteria importance through the inter-criteria correlation (CRITIC) method and non-dominated sorting genetic algorithm based on the grid partitioning (NSGA-G) are applied to compute the weights of responses and find optimality. The optimal outcomes of the S, D, f, and DT were 370 rpm, 0.10 mm, 0.04 mm/rev, and 8 mm, respectively. The improvements in the Ra and VH were 40.7 % and 7.6 %, respectively, as compared to the original parameters. An effective approach combining the BRFFNN, CRITIC, and NSGA-G can be widely utilized to deal with complicated optimization problems. The optimizing results can be employed to enhance the surface properties of the burnished surface.
Keywords: single diamond burnishing; average roughness; Vickers hardness; Bayesian regularization; NSGA-G

Highlights
- *A new diamond burnishing operation combining the minimum quantity lubrication (MQL) system and vortex tubes was developed.*
- *Process parameters, including the spindle speed, depth of penetration, feed rate, and diameter of the tool tip were optimized.*
- *The average roughness and Vickers hardness of the burnished surface were enhanced.*
- *Optimal Bayesian regularized feed-forward neural network was proposed to present the non-linear data.*

0 INTRODUCTION

In industrial applications, the cost of lubricants accounts for 7 % to 17 % of the production expense. Moreover, the usage of the cutting fluid causes health risks and environmental problems; hence, the reduction or elimination of the lubricants is necessary. For this purpose, various cooling-lubrication (CL) approaches, including the minimum quantity lubrication (MQL), the Vortex tube (VT), and the cryogenic approach have been developed and utilized.

The deployment of the MQL system for different machining processes has attracted many researchers. Zaman and Dhar [1] stated that Ra, cutting force (CF), and cutting temperature (CT) were decreased by 5.78 %, 1.27 %, and 3.93 % at a proper parameter setting, respectively, for the MQL turning Ti6Al4V, in which the nozzle diameter, nozzle elevation angle (A), flow rate (Q), and air pressure were optimizing inputs. Tamang et al. [2] emphasized that the power consumption (PC), Ra, and tool wear (TW) of the MQL turning Inconel 825 were decreased by 16.57 %, 8.47 %, and 10.41 %, respectively, as compared to the dry condition. Moreover, the Ra of 0.49 μm, the PC of 5.44 kW, and the TW of 110.68 μm were obtained

at the optimal condition. Zan et al. [3] stated that CT, CF, and acceleration were decreased by 150 ºC, 5.6 %, and 8.9 %, respectively using optimal values of the Q, nozzle distance (N), and A for the MQL milling Ti6Al4V. The Ra of 0.32 μm, the CT of 103.8 ºC, and the CF of 115.1 N for the MQL milling Inconel 690 were obtained by means of optimal parameters of the S, f, depth of cut (dc), Q, and A [4]. Van and Nguyen [5] presented that the cylindricity, circularity, and average roughness of the MQL roller burnishing were reduced by 53.2 %, 57.8 %, and 72.9 %, respectively with the support of the optimal data of the nozzle diameter, A, Q, and air pressure. The maximum roughness and VH of the MQL roller burnishing were decreased by 17 % and 14 %, respectively using the ANN and PSO [6]. Sachin et al. [7] developed an MQL diamond-burnishing process, in which the optimal outcomes of the Ra and VH were 0.07 μm and 363 HV, respectively using the optimal data of the S, f, and burnishing force (f_b).

The VT has been widely utilized to enhance the technical performances of various machining processes. Mahapatro and Krishna [8] revealed that the CT and Ra of the VT-based turning Ti-6Al-4V were decreased by 35.6 % and 66.14 %, respectively,

*Corr. Author's Address: Nguyen Tat Thanh University, 300A Nguyen Tat Thanh, Ho Chi Minh, Vietnam, lvan@ntt.edu.vn

155

while the *CF* was increased by 18.6 %, as compared to the dry cutting. Singh et al. [9] emphasized that the VT caused 45 % to 56 % lower carbon emission for the turning Ti-3Al-2.5V in comparison with the dry condition. Gupta et al. [10] proposed an effective system VTMQL comprising the nitrogen, VT, and MQL to increase the machinability in the turning of AA 7075-T6 alloy, in which the *TW* and *Ra* were decreased by 118 % and 77 %, respectively. Similarly, Mia et al. [11] revealed that the VTMQL caused reductions in the *TW* and *Ra* around 72 % and 75 %, respectively, for the precision turning of Al 6061-T6. The *CF* and *Ra* of the VTMQL-based drilling Hardox 500 steel were decreased by 36.8 % and 46.7 %, respectively, as compared to the MQL, while the *TW* decreased around 4.5 times in comparison with the dry condition [12].

The cryogenic method has been considered for different machining processes. Sharma et al. [13] stated that the *CF* of 44.49 N, the *CT* of 24.99 ºC and the machining time of 37.09 s were obtained at the optimal data for the cryogenic turning AISI D3 using the Taguchi method. The specific cutting energy (*SCE*), *Ra,* and *TW* for the cryogenic turning Ti-6Al-4V were decreased by 30.5 %, 22.8 %, and 4.3 %, respectively, as compared to the dry condition [14]. The *S* of 78 m/min, the *f* of 0.16 mm/rev, and SNMM tool insert could be applied to decrease the *Ra* (1.05 μm) and the *CF* (315 N) for the cryogenic turning Ti-

6Al-4V [15]. The optimal values of the *S*, *f*, and f_b of the cryogenic diamond burnishing operation were 73 m/min, 0.048 mm/rev, and 150 N, respectively for decreasing the *Ra* and improving the *VH* [16]. Sachin et al. [17] stated that *Ra* of 0.2 μm and the *VH* of 398 HV for the diamond burnishing operation of the 17-4 hardened stainless could be obtained using optimal outcomes.

The diamond burnishing process is one of the finest finishing technologies, which has been widely executed on different surfaces for improving the properties and working functionalities [18] to [20]. Various CL methods, including cryogenic and MQL conditions, have been utilized in various diamond-burnishing operations. Unfortunately, the cryogenic approach requires an expensive investment, while the low cooling-lubrication impact is the greatest drawback of the MQL system when machining high- hardness steels due to the enormous amount of generated heat. Therefore, it is necessary to develop an efficient-economic cooling-lubrication approach that can effectively facilitate the diamond-burnishing process.

Additionally, the selection of optimal factors for improving the surface quality of the diamond burnishing under the impact of a new CL system is also an urgent demand.

In this paper, a new diamond burnishing operation comprising the MQL and double vortex tubes is
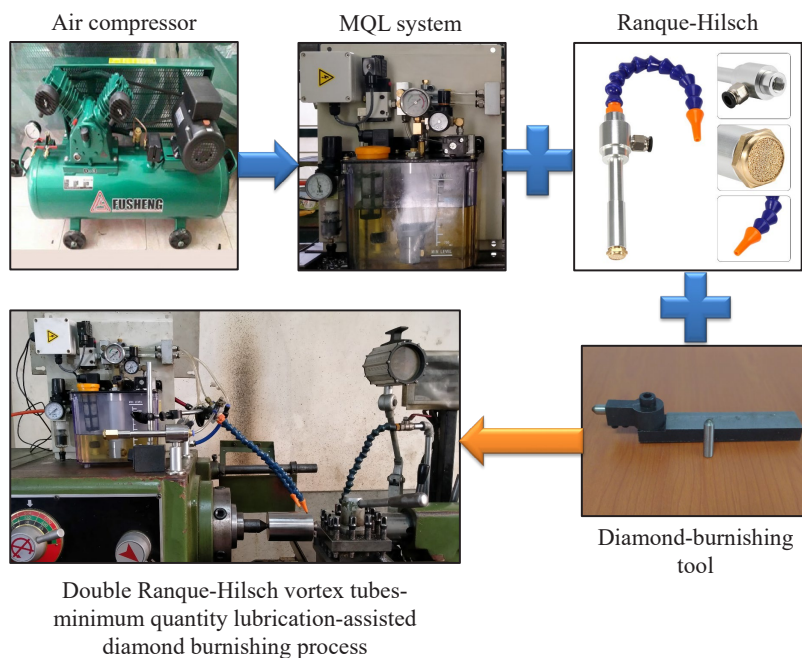

Double Ranque-Hilsch vortex tubes-
minimum quantity lubrication-assisted
diamond burnishing process

Fig. 1. *A new diamond-burnishing process*

first introduced. Then, we present the optimization approach and experiment. Next, the obtained results are discussed. Finally, conclusions are drawn, and future research is suggested.

1 NEW DIAMOND-BURNISHING PROCESS

The concept of the diamond burnishing operation with a new CL system is shown in Fig. 1. The compressed air is produced by the pneumatic pump and stored in the accumulator. The pressure value is detected and assigned using the pneumatic regulator valve. The lubricant is pumped by means of the electrical device, while the flow rate is adjusted using the frequency generator. The compressed air is transferred from the MQL system to the double vortex tubes for decreasing the working temperature. The cold mixture is produced and transferred into the burnishing regions.

Table 1. *Optimizing parameters of a new diamond burnishing process*

Symbol	Parameters	1	2	3
S	Spindle speed [rpm]	185	370	630
D	Depth of penetration [mm]	0.06	0.08	0.10
f	Feed rate [mm/rev]	0.04	0.06	0.08
DT	Tool-tip Diameter [mm]	6	8	10

2 OPTIMIZATION APPROACH

The burnishing parameters, including the spindle speed (S), depth of penetration (D), feed rate (f), and tool-tip diameter (DT) are presented in Table 1. The ranges of the S, D, and f are determined based on the characteristics of the machine tool, while the DT value is selected using the characteristics of the burnishing tool. Consequently, the optimizing issue is expressed as:

Minimize the Ra and maximize the VH.

Constraints: 150 rpm $\leq S \leq$ 630 rpm; 0.06 mm $\leq D \leq$ 0.10 mm; 0.04 mm/rev $\leq f \leq$ 0.08 mm/rev; 8 mm $\leq DT \leq$ 10 mm.

The optimizing approach is expressed in Fig. 2.

Step 1: The experimental data are observed using the Taguchi method.
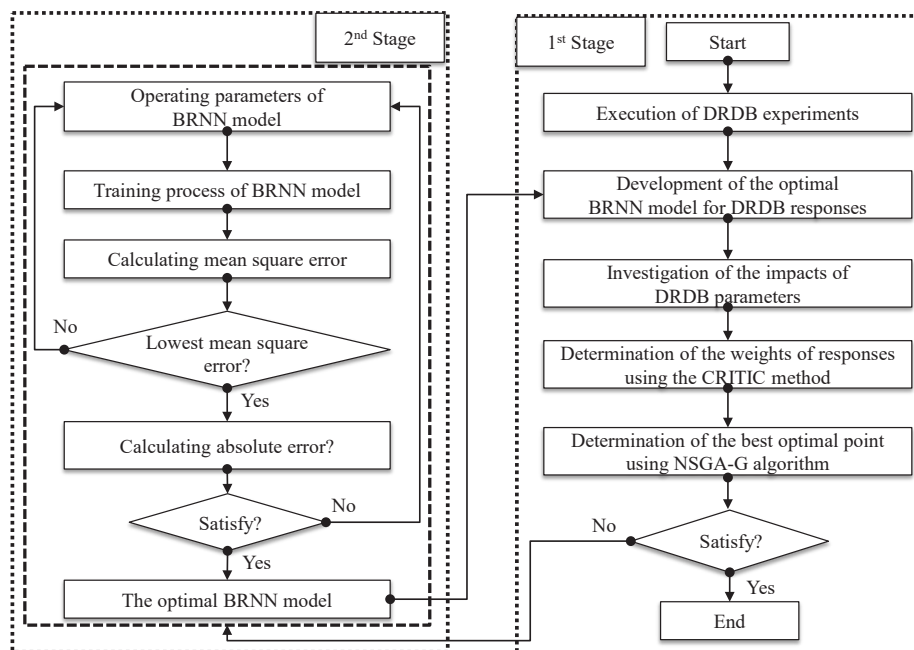
The Ra value is calculated as:

$$Ra = \frac{\sum_{i=1}^{n} Ra_i}{n}, \qquad (1)$$

where Ra_i denotes the average roughness at the ith measured location.

The VH value is calculated as:

$$VH = \frac{\sum_{i=1}^{n} VH_i}{n}, \qquad (2)$$

where VH_i is the Vickers hardness at the ith position.

Fig. 2. *The optimizing procedure*

Step 2: The *Ra* and *VH* models are developed using the BRFFNN approach [21].

The input parameters are considered as probability density functions to the hidden layer, which is expressed as:

$$P = \frac{P(D|w,\beta,M)P(w|\alpha,M)}{P(D|\alpha,\beta,M)}, \qquad (3)$$

where D and M presents the obtained data and the forward multi-layer perceptron, respectively. w and $P(w|\alpha,M)$ are the vector and prior knowledge of network weights, respectively. When the Gaussian function is employed, the likelihood-$P(D|w, \beta, M)$ is expressed as:

$$P(D|w,\beta,M) = \frac{1}{\left(\pi/\beta\right)^{n/2}} e^{-\beta d_d}, \qquad (4)$$

where d_d is the sum of squared deviations for data.

The normalized factor $P(D|\alpha, \beta, M)$ is expressed as:

$$P(D|\alpha,\beta,M) = \frac{1}{\left(\pi/\alpha\right)^{N/2}} e^{-\alpha d_w}, \qquad (5)$$

where d_w is the sum of squared errors for the weights.

The probability density function can be expressed as:

$$P = \frac{1}{Z_F(\alpha,\beta)} e^{-(\beta d_d + \alpha d_w)}. \qquad (6)$$

The highest posterior probability density function causes maximum regularized objective function ($f = \beta d_d + \alpha d_w$).

To observe the optimal architecture of the BRFFNN model, the operating factors, including the number of neurons in each layer, performance function, transfer function, number of hidden layers, and learning functions are optimized and selected. The numerical experiments of each ANN model are executed to calculate the mean square error (*MSE*), which is expressed as:

$$MSE = \frac{1}{N} \sum_{i=1}^{N} \left(y_a - y_p\right)^2, \qquad (7)$$

where y_a and y_p are the actual and predictive values, respectively. N denotes the number of testing points.

The best BRFFNN architecture is chosen with the lowest MSE value.

Step 3: The weights of the machining responses are calculated using the criteria importance through the intercriteria correlation (CRITIC) method.

The normalized burnishing response (x_{ij}) is computed as:

$$x_{ij} = \frac{x_{ij} - x_j^{word}}{x_j^{best} - x_j^{word}}. \qquad (8)$$

The standard deviation (s_j) of each response is calculated as:

$$s_j = \sqrt{\frac{\left(\sum_{i=1}^{m} x_{ij} - x_m\right)^2}{m-1}}. \qquad (9)$$

Determination of symmetric matrix of $n \times n$ with element r_{jk}, which is linear correlation coefficient between the vectors x_j and x_k.

Computation of measure of the conflict (I_j):

$$I_j = \sum_{k=1}^{m} (1 - r_{jk}). \qquad (10)$$

Determination of the quantity of the information (C_j):

$$C_j = s_j \sum_{k=1}^{m} (1 - r_{jk}). \qquad (11)$$

The computed (w_i) of burnishing response is calculated as:

$$w_i = \frac{C_j}{\sum_{k=1}^{n} C_j}. \qquad (12)$$

Step 4: The optimal data of the burnishing parameters and responses are selected using the non-dominated sorting genetic algorithm based on the grid partitioning (NSGA-G) [22]. The operation steps of the NSGA-G are expressed in Fig. 3.
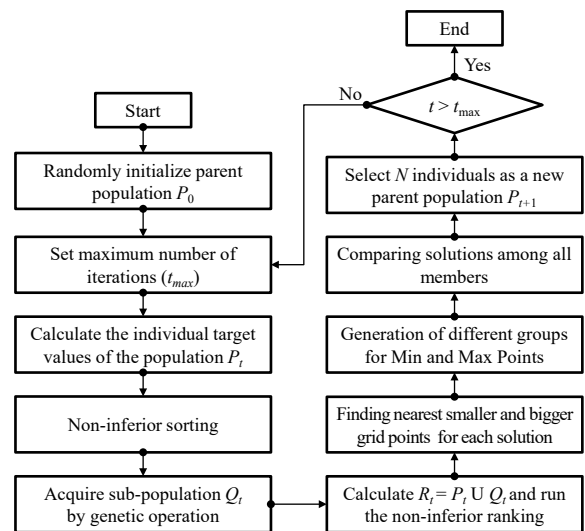

Fig. 3. *The working principle of the NSGA-G*

The random initialization of parent population: the parent population is executed based on the definition of the optimizing issue.

Non-dominance sorting of the parent population: the parent population (P) is divided into the number of the subsets (P_i), in which the subset P_{k+1} is dominated by the individual P_k. The individual P_i is expressed as:

$$P_i = \left\{ i / n_i, i \in \left\{ 1, 2, ..., N \right\} \right\}. \qquad (13)$$

The population P_k is expressed as:

$$P_k = \left\{ \text{All individual} / n_i - \text{k} + 1 \right\}, \qquad (14)$$

where n_i is the number of individuals in the population for dominating generations.

The parent population with N size and offspring population with N members at tth generation are produced with the aid of crossover and mutation operations.

Generation of different groups for Min and Max Points: the nearest smaller and bigger grid point for each solution were selected. The design space is divided into multi small groups.

Compare solutions in a group and selection of the best individual: The weak individuals are removed to form a new generation. The control loop is executed until the maximum number of generations is fit.

3 EXPERIMENTAL SETTING

The machining specimens having the round cylindrical shape are made from the hardened AISI 4340 steel. The length and diameter of each workpiece are 130 mm and 80 mm, respectively. The turning and grinding operations are applied to produce the external surface in each specimen. The average roughness and Vickers hardness of the pre-machined surface are approximately 2.46 µm and 420.6 HV, respectively.

The experiments are performed using a conventional turning machine. The dead and live centres are employed to hold the specimen (Fig. 4a). The rotational motion of the workpiece is conducted by means of the friction between the machining sample and the dead centre.

A novel diamond-burnishing tool has been designed and fabricated to facilitate burnishing experiments, as shown in Fig. 4b. Primary components are the shank, tool head, stem, diamond tip, positioning bolts, and adjusting screws. The stem having the diamond tip is tightly mounted in the tool head. The stem is replaced after each experiment to eliminate the impact of the tool wear. The hardness of 62 HRC and roughness of 0.05 µm are employed in the diamond tip.

The average roughness is computed from three different positions using the Mitutoyo SJ-301. The

Vickers hardness is measured in three different points on the burnished surface using a Wilson Wolpert tester.

The representative values of the burnishing responses are presented in Fig. 5.
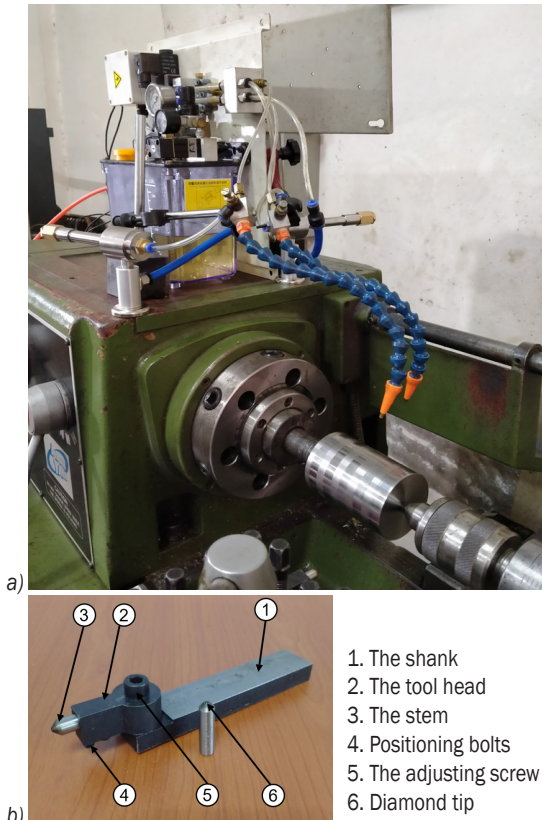
4 RESULTS AND DISCUSSIONS

4.1 Impacts of Process Parameters on the Ra and VH

Table 2 presents experimental data for the diamond burnishing operation.

Table 2. *Experimental data for a new diamond burnishing process*

	No.	S	D	f	DT	Ra	VH
	1	185	0.06	0.04	6	0.46	511.5
	2	370	0.06	0.06	6	0.42	478.3
	3	630	0.06	0.08	6	0.44	424.6
	4	370	0.06	0.04	8	0.31	488.8
	5	630	0.06	0.06	8	0.32	451.6
	6	185	0.06	0.08	8	0.54	480.2
	7	630	0.06	0.04	10	0.23	444.4
	8	185	0.06	0.06	10	0.42	484.8
	9	370	0.06	0.08	10	0.41	456.2
	10	370	0.08	0.04	6	0.27	497.7
	11	630	0.08	0.06	6	0.29	464.8
Experimental data for developing the BRNN model	12	185	0.08	0.08	6	0.54	474.3
	13	630	0.08	0.04	8	0.18	475.7
	14	185	0.08	0.06	8	0.41	496.6
	15	370	0.08	0.08	8	0.38	469.9
	16	185	0.08	0.04	10	0.29	485.1
	17	370	0.08	0.06	10	0.27	474.3
	18	630	0.08	0.08	10	0.33	446.8
	19	630	0.10	0.04	6	0.14	495.7
	20	185	0.10	0.06	6	0.39	497.3
	21	370	0.10	0.08	6	0.37	472.4
	22	185	0.10	0.04	8	0.26	503.8
	23	370	0.10	0.06	8	0.24	494.8
	24	630	0.10	0.08	8	0.29	470.9
	25	370	0.10	0.04	10	0.13	483.1
	26	630	0.10	0.06	10	0.18	475.7
	27	185	0.10	0.08	10	0.36	481.8
	28	185	0.06	0.05	7	0.46	505.4
	29	250	0.07	0.07	9	0.41	481.9
Experimental data for testing the precision of the BRNN model	30	250	0.09	0.05	7	0.32	501.3
	31	630	0.10	0.07	9	0.23	477.6
	32	370	0.07	0.06	10	0.31	470.5
	33	250	0.08	0.08	9	0.41	476.9
	34	185	0.06	0.05	9	0.41	496.3
	35	370	0.08	0.07	7	0.36	477.9
	36	370	0.06	0.06	8	0.37	479.4

Fig. 4. *The experimental setting; a) burnishing experiment, and b) diamond burnishing tool*

1. The shank
2. The tool head
3. The stem
4. Positioning bolts
5. The adjusting screw
6. Diamond tip

The machining time available to process material decreases with an increased f; hence, the Ra increases.
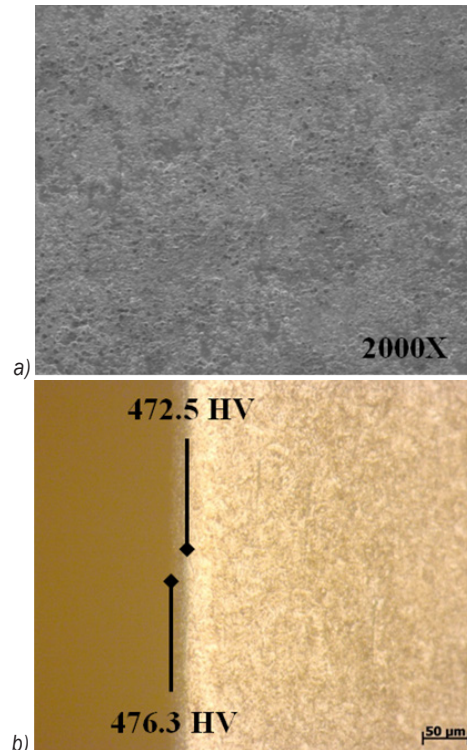
Fig. 5. *The representative values of a new diamond-burnishing process; a) the SEM image of the burnished surface at the experimental No. 11, and b) the Vickers hardness at the experimental No. 11*

As shown in Fig. 6a, the Ra decreases (relatively around 34.8 %) with an increase in the S (from 185 rpm to 630 rpm). Higher S increases the engagement frequency between the diamond tip and the surface, which increases the number of burnishing traces. The irregularities of the pre- machined surface are easily deformed; thus, the Ra decreases. The machining temperature at the interfaces increases with an increased S, which reduces the hardness and strength of the workpiece; hence, the material is smoothly compressed. Therefore, a reduction in the Ra is obtained.

As shown in Fig. 6b, an increase in the D (from 0.06 mm to 0.10 mm) leads to a reduction in the Ra (relatively around 30.4 %). Higher D increases the machining pressure on the surface to be machined, and the material is compressed. The pre-machined peaks are flattened, and the valleys are filled up; hence, the Ra significantly decreases.

As shown in Fig. 6c, an increase in the f (from 0.04 mm/rev to 0.08 mm/rev) increases the Ra (relatively around 24.4 %). An increased f causes a higher distance between the consecutive burnishing paths, which decreases the engagement frequency.

As shown in Fig. 6d, an increase in the DT (from 8 mm to 10 mm) decreases the Ra (relatively around 19.6 %). An increased DT causes a higher contact length between the tool tip and the specimen's surface. The pre-machined peaks are flattened, and the valleys are filled up; thus, the Ra significantly decreases.

Table 3. *Computed ANOVA results for the Ra*

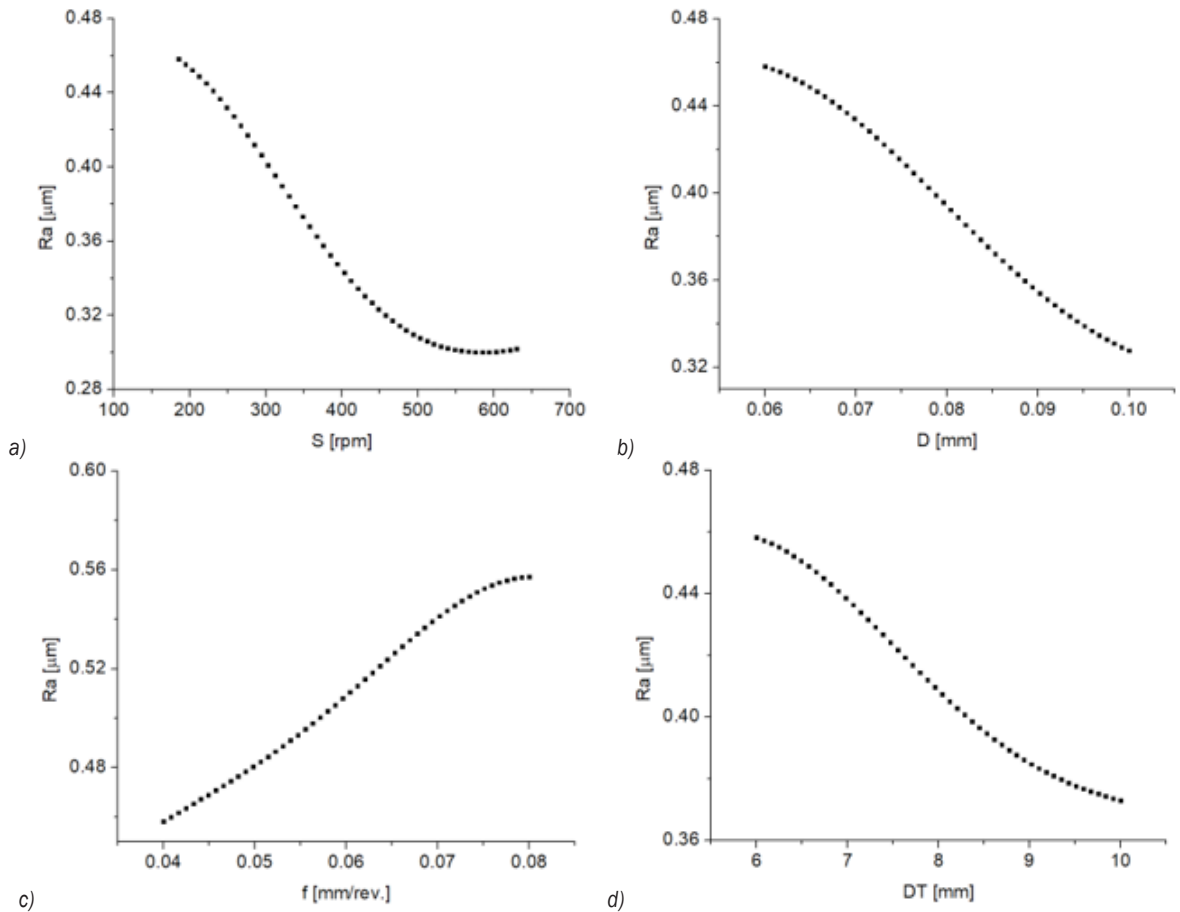| Source	SS	MS	F value	p-value
Model	0.209	0.015	41.916	< 0.0001
S	0.178	0.178	499.782	< 0.0001
D	0.164	0.164	458.560	< 0.0001
f	0.197	0.197	552.648	< 0.0001
DT	0.094	0.094	264.563	< 0.0001
Sf	0.013	0.013	35.166	0.0182
SDT	0.038	0.038	105.732	0.0091
S^2	0.103	0.103	288.085	< 0.0001
DT^2	0.015	0.015	42.619	0.0174
Residual	0.004	0.000		
Cor. total	0.213			
R^2 = 0.9816; Adjusted R^2 = 0.9724; Predicted R^2 = 0.9682				

Fig. 6. *Parametric influences on the Ra; a) Ra vs. S, b) Ra vs. D, c) Ra vs. f, and d) Ra vs. DT*

The contribution of each factor on the *Ra* is shown in Table 3. Significant parameters are all single factors (*S*, *D*, *f*, and *DT*), interactive factors (*Sf* and *SDT*), and quadratic factors (S^2 and DT^2). The contributions of the *S*, *D*, *f*, and *DT* are 21.46 %, 19.69 %, 23.73 %, and 11.36 %, respectively. The contributions of the *Sf* and *SDT* are 1.51 % and 4.54 %, respectively. The contributions of the S^2 and DT^2 are 12.37 % and 1.83 %, respectively. The R^2 value of 0.9816 indicates the *Ra* model is adequate.

As shown in Fig. 7a, the *VH* decreases (relatively around 12.3 %) with an increased *S* (from 105 rpm to 630 rpm). An increase in the *S* increases the engagement frequency, leading to higher machining temperature at the burnishing area; hence, the *VH* decreases.

As shown in Fig. 7b, an increased *D* (from 0.06 mm to 0.10 mm) leads to a higher *VH* (relatively around 2.5 %). An increased *D* increases the machining pressure on the surface to be machined.

The material is compressed and higher *VH* is obtained.

As shown in Fig. 7c, an increased higher *f* (from 0.04 mm/rev to 0.08 mm/rev) decreases the *VH* (relatively around 9.8 %). A higher *f* causes a low degree of plastic deformation due to higher distance among the consecutive traces; hence, the *VH* decreases.

As shown in Fig. 7d, an increased *DT* (from 6 mm to 10 mm) decreases the *VH* (relatively around 6.1 %). At a lower *DT*, higher burnishing pressure is produced due to the low contact area between the tool tip and surface to be machined. More material is compressed and the *VH* increases. When the *DT* increases, the burnishing pressure decreases; hence, the *VH* decreases.

The contribution of each factor on the Vickers hardness is shown in Table 4. Significant parameters are all single factors (*S*, *D*, *f*, and *DT*), interactive factors (*SD*, *Sf*, *SDT*, *DDT*, and *fDT*), and quadratic factors (S^2, D^2, f^2, and DT^2). The contributions of the
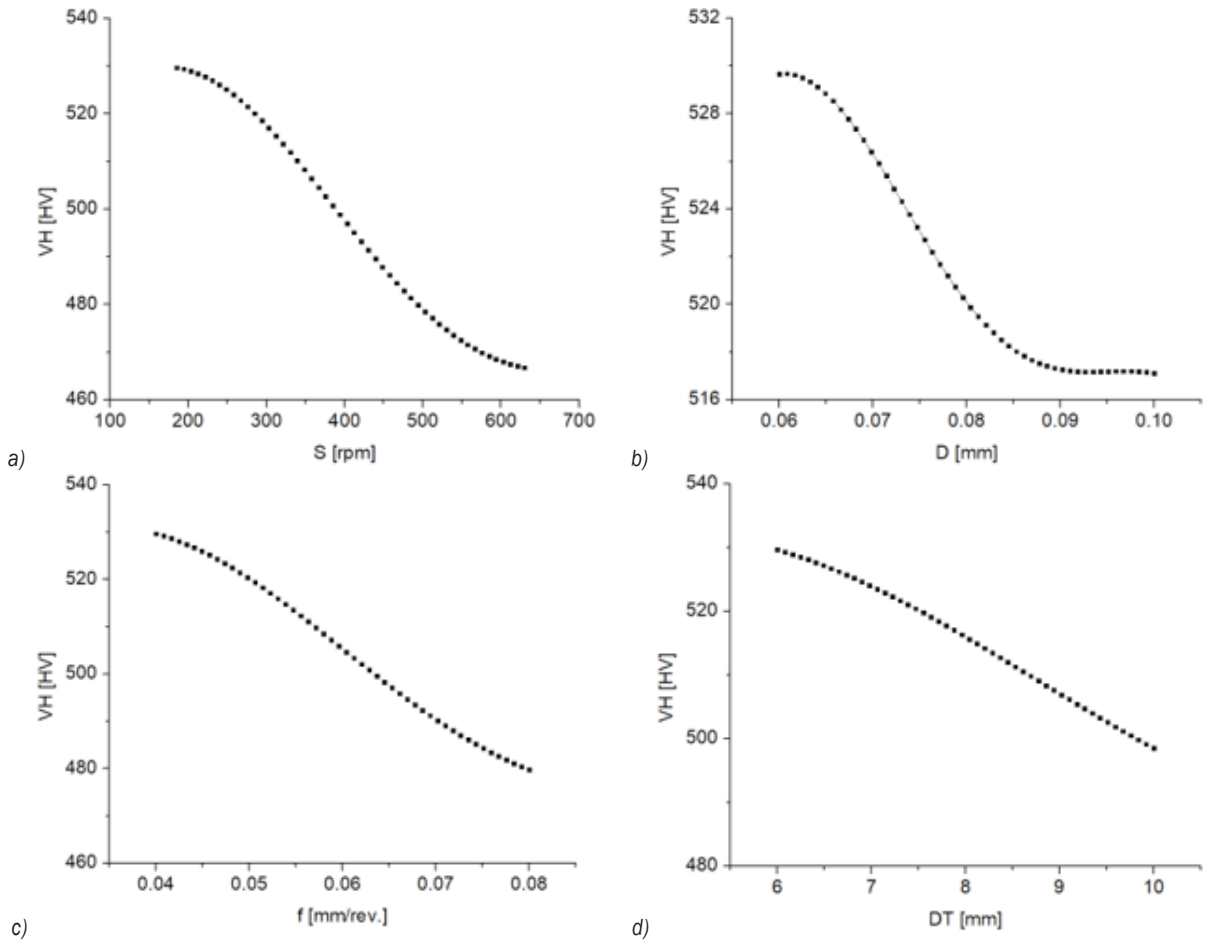
Fig. 7. *Parametric influences on the VH; a) VH vs. S, b) VH vs. D, c) VH vs. f, and d) VH vs. DT*

S, D, f, and DT are 19.51 %, 12.79 %, 16.31 %, and 8.77 %, respectively. The contributions of the SD, Sf, SDT, DDT, and fDT are 10.0 %, 1.25 %, 3.75 %, 1.68 %, and 11.19 %, respectively. The contributions of the S^2, D^2, f^2, and DT^2 are 1.82 %, 2.33 %, 4.44 %, and 5.48 %, respectively. The R^2 value of 0.9843 indicates the developed VH model is adequate.

4.2 Impacts of MQL Parameters on the Ra and VH

The ranges of the flow rate (Q), nozzle distance (N), and nozzle elevation angle (A) are selected based on the characteristics of the MQL system and confirmed with references [1], [3], and [5]. The Box-Benkhen design with two replications is applied to produce the experimental data in terms of saving trial costs and human efforts, as shown in Table 5.

As shown in Fig. 8a, when the Q relatively increases from 40 ml/h to 120 ml/h, the Ra is relatively decreased by 39.5 %. A higher Q increases the number

Table 4. *Computed ANOVA results for the VH*

Source	SS	MS	F value	p-value
Model	7624.43	544.60	49.26	< 0.0001
S	1856.20	1856.20	167.90	< 0.0001
D	1216.86	1216.86	110.07	< 0.0001
f	1551.75	1551.75	140.36	< 0.0001
DT	834.39	834.39	75.47	< 0.0001
SD	951.41	951.41	86.06	0.0002
Sf	118.93	118.93	10.76	0.0014
SDT	356.78	356.78	32.27	0.0006
DDT	64.70	64.70	5.85	0.0012
fDT	159.84	159.84	14.46	< 0.0001
S^2	1064.63	1064.63	96.30	0.0011
D^2	173.16	173.16	15.66	0.0008
f^2	221.68	221.68	20.05	0.0005
DT^2	422.43	422.43	38.21	0.0004
Residual	521.37	521.37	47.16	
Cor. total	121.61	11.06		
$R^2 = 0.9843$; Adjusted $R^2 = 0.9752$; Predicted $R^2 = 0.9636$				

of oil droplets entering the burnishing zone, which enhances the cooling-lubrication efficiency. The friction at the interfaces decreases and the burnished surface is wetted and protected; hence, the Ra significantly decreases.
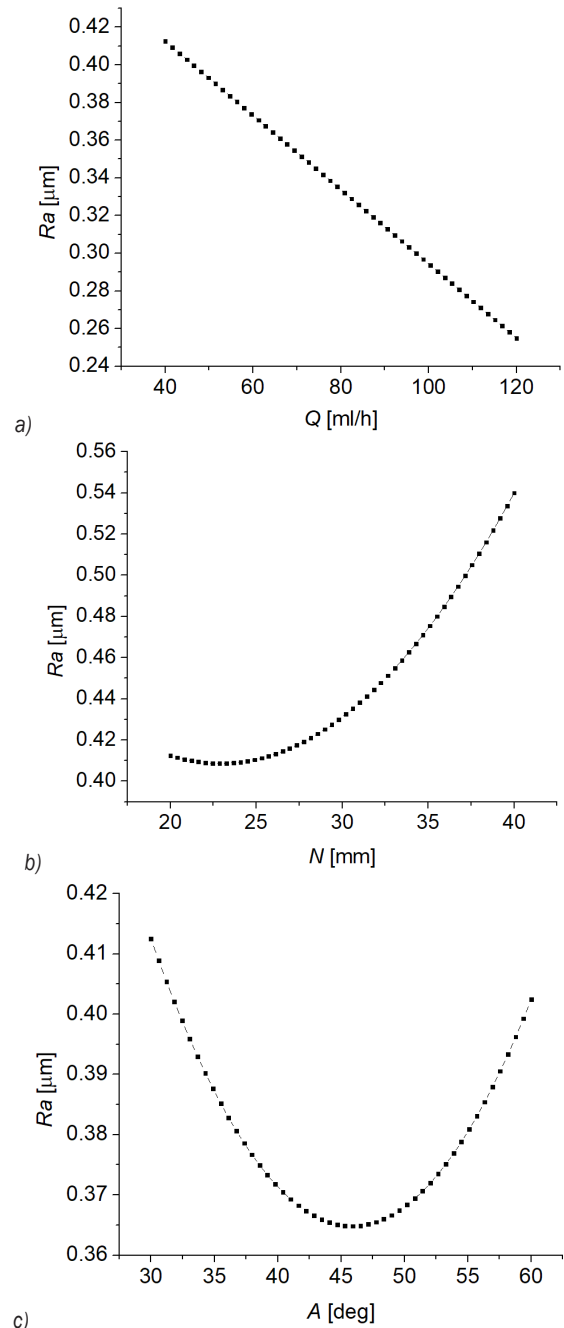
Table 5. *The impacts of MQL parameters on the Ra and VH*

No.	Q [ml/h]	N [mm]	A [deg]	Ra [μm]	VH [HV]
1	40	30	60	0.41	451.8
2	80	40	60	0.33	459.2
3	120	30	30	0.29	491.2
4	80	40	30	0.33	457.1
5	120	30	60	0.28	492.8
6	80	30	45	0.31	485.2
7	40	30	30	0.43	450.4
8	40	40	45	0.37	448.4
9	80	30	45	0.31	484.2
10	80	20	60	0.46	492.9
11	120	20	45	0.35	513.8
12	120	40	45	0.21	478.6
13	80	30	45	0.31	486.8
14	40	20	45	0.49	468.2
15	80	20	30	0.47	491.8

As shown in Fig. 8b, when the N relatively increases from 20 mm to 40 mm, the Ra is relatively increased by 30.9 %. At a low distance, a high proportion of the mixture is effectively transferred into the burnishing zones, resulting in low friction at the interfaces. The cooling-lubrication efficiency improves; thus, the Ra decreases. When the distance increases, a low proportion of the mixture enters into the burnishing zones, resulting in a lower cooling-lubrication efficiency; hence, the Ra increases.

As shown in Fig. 8c, a higher A causes a reduced Ra value, while a further angle causes a negative impact. When the angle increases from 30 deg to 45 deg, the Ra is relatively decreased by 13.8 %. When the angle increases from 45 deg to 60 deg, the Ra is relatively increased by 12.9 %. An increased angle leads to a decreased Ra due to a reduction in friction with the aid of proper positions of nozzles. However, a further increased angle causes a higher frictional impact at the interfaces and the Ra slightly increases.
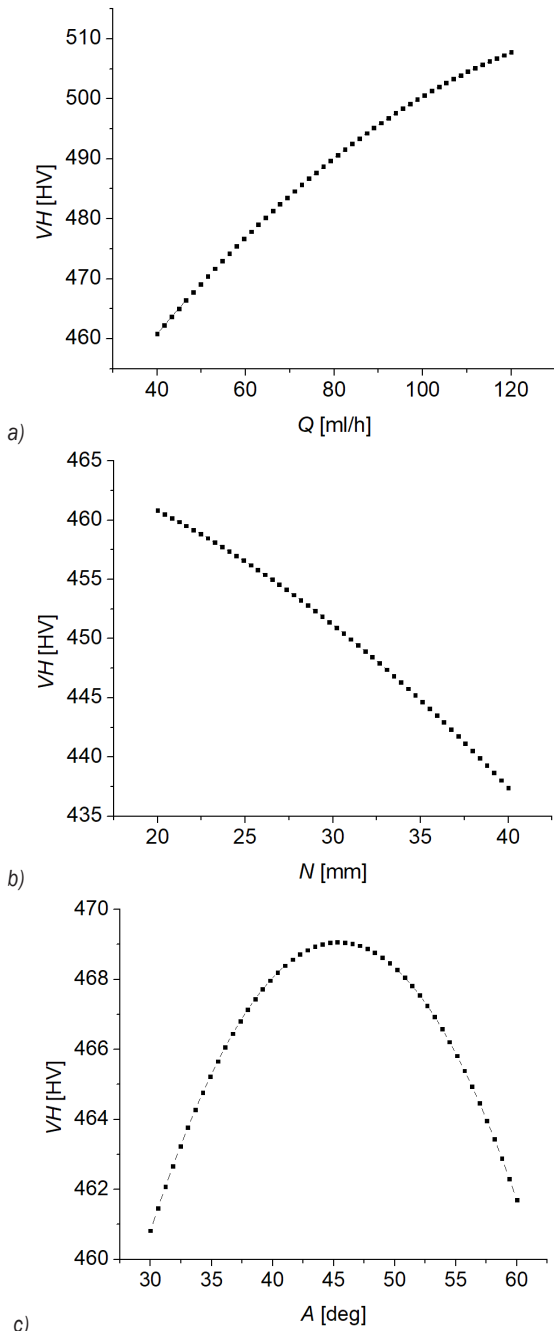
As shown in Fig. 9a, when the Q relatively increases from 40 ml/h to 120 ml/h, the VH is enhanced by 10.8 %. An increased Q leads to a higher amount of lubricant; thus, the burnished surface is wetted and protected. The friction at the interface decreases, leading to a reduction in the machining temperature. The diminishing of the residual stress is then prevented; thus, a higher VH is achieved.

a)

b)

c)

Fig. 8. *Impacts of MQL parameters on the Ra;*
a) Ra vs. Q, b) Ra vs. N, and c) Ra vs. A

As shown in Fig. 9, when the N relatively increases from 20 mm to 40 mm, the VH is relatively decreased by 6.2 %. At a low distance, a higher amount of lubricant enters into the burnishing zone, which wets and protects the burnished surface. The machining temperature at the interfaces decreases, which diminishes the residual stress; hence, the VH enhances. At a low distance, the temperature at the

interfaces increases, leading to diminishing residual stress; hence, the *VH* decreases.

a)

b)

c)

Fig. 9. *Impacts of MQL parameters on the VH; a) VH vs. Q, b) VH vs. N, and c) VH vs. A*

As shown in Fig. 9c, the contradictory trends of the *VH* are observed under the variety of the elevation angle. When the angle increases from 30 deg to 45 deg, the *VH* is relatively improved by 1.7 %. When the elevation angle increases from 45 deg to 60 deg, the

VH is relatively reduced by 1.5 %. An increased angle causes an accurate penetration of the mixture, leading to a reduction in the machining temperature; thus, a higher *VH* is obtained. A further increased angle leads to an improper cooling-lubrication efficiency, resulting in a higher burnishing temperature and the residual stress is relieved; hence, the *VH* decreases.

4.3 Optimal BRNN Model

The operating parameters of the BRFFNN model, including the *HN*, *PM*, *TF*, *HL*, and *LF* are shown in Table 6. The computational trials of the BRFFNN are performed based on the parameter combination entitled Taguchi L_{18}. The obtained results of the *MSE* values are shown in Table 7. As a result, the optimal data of the *HN*, *PM*, *TF*, *HL*, and *LF* are 19, MSEREG, logsig, 3, and LearnGDM, respectively. The schematic of the developed BRNN model is presented in Fig. 10.

To confirm the precision of the developed ANN model, the comparisons between the experimental and predictive results are conducted. Table 8 indicates the comparative values at different points. As a result, the computed deviations of the *Ra* and *VH* lie from -313 % to 4.35 % and -0.52 % to 0.65 %, respectively. The small errors revealed that the proposed models ensure the prediction accuracy.
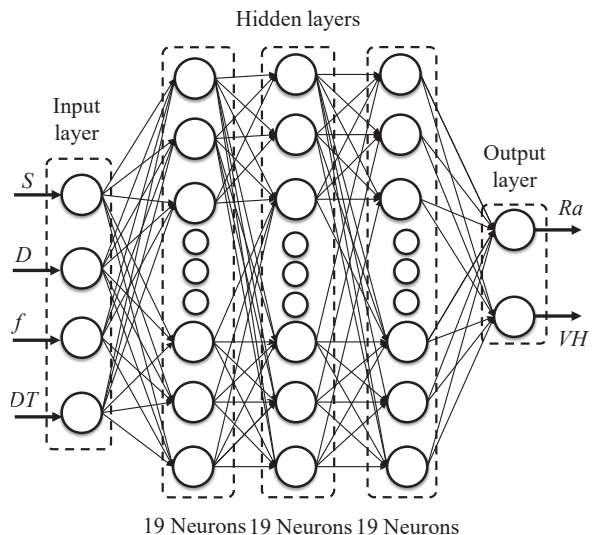
Fig. 10. *The schematic of the developed BRNN model*

The regression plots of the BRFFNN are depicted in Fig. 11, in which the *R* values of the training, testing, and all stages are 0.97364, 0.96032, and 0.96536, respectively. Consequently, the developed BRFFNN model can accurately approximate experimental data.

**Table 6.** *Operating parameters of the BRNN model*

Symbol	Parameters	Classifications
HN	Number of hidden neurons	15 to 20
PM	Performance function	Mean squared error: MSE; Mean squared error with regularization: MSEREG; Sum squared error: SSE
TF	Transfer function	Log sigmoid: logsig; Linear: purelin; Hyperbolic tangent sigmoid: tansig
HL	Number of hidden layers	1; 2; 3
LF	Learning function	Gradient descent with momentum weight and bias learning function: LearnGDM; Gradient descent weight and bias learning function: LearnGD

Table 7. *Computing the MSE values*

No.	HN	PM	TF	HL	LF	MSE
1	15	MSE	logsig	1	LearnGDM	0.004236
2	15	MSEREG	purelin	2	LearnGD	0.002298
3	15	SSE	tansig	3	LearnGDM	0.001948
4	16	MSE	logsig	2	LearnGD	0.001481
5	16	MSEREG	purelin	3	LearnGDM	0.000929
6	16	SSE	tansig	1	LearnGDM	0.001025
7	17	MSE	purelin	1	LearnGDM	0.000622
8	17	MSEREG	tansig	2	LearnGDM	0.00106
9	17	SSE	logsig	3	LearnGD	0.001016
10	18	MSE	tansig	3	LearnGD	0.001477
11	18	MSEREG	logsig	1	LearnGDM	0.000653
12	18	SSE	purelin	2	LearnGDM	0.006799
13	19	MSE	purelin	3	LearnGDM	0.000606
14	19	MSEREG	tansig	1	LearnGD	0.000632
15	19	SSE	logsig	2	LearnGDM	0.00066
16	20	MSE	tansig	2	LearnGDM	0.006992
17	20	MSEREG	logsig	3	LearnGDM	0.001112
18	20	SSE	purelin	1	LearnGD	0.007437

Table 8. *Investigation of the precision of the developed BRNN model*

No.	Ra			VH		
	Experiment	BRFFNN	Error [%]	Experiment	BRFFNN	Error [%]
28	0.46	0.47	-2.17	505.4	504.6	0.16
29	0.41	0.42	-2.44	481.9	480.6	0.27
30	0.32	0.33	-3.13	501.3	503.9	-0.52
31	0.23	0.22	4.35	477.6	479.9	-0.48
32	0.31	0.32	-3.23	470.5	468.4	0.45
33	0.41	0.42	-2.44	476.9	473.8	0.65
34	0.41	0.42	-2.44	496.3	498.7	-0.48
35	0.36	0.35	2.78	477.9	475.8	0.44
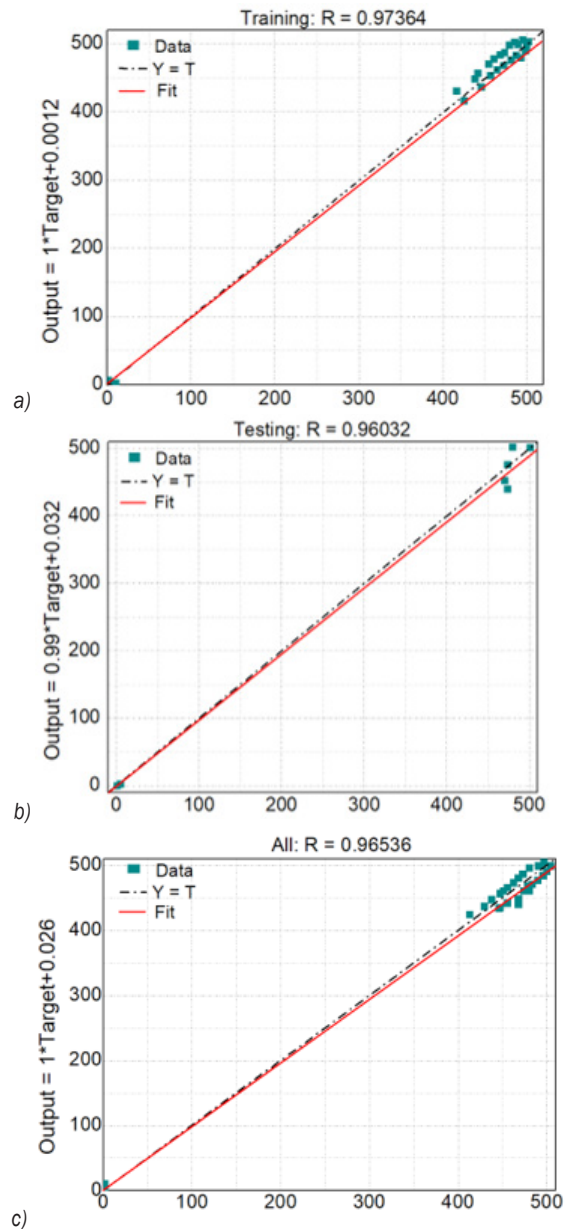
Fig. 11. *Regression plots for the BRNN model; a) training stage, b) testing stage, and c) all stages*

4.4 Optimizing outcomes

The computed weights of the *Ra* and *VH* are 0.53 and 0.47, respectively. To prove the effectiveness of the NSGA-G, the optimal data produced by NSGA-II are generated and compared. Fig. 12 presents the Pareto front produced by the NSGA-G. The computational times of the NSGA-G and NSGA-II are 80.8 s and 126.4 s, respectively. The number of feasible designs produced by the NSGA-G and NSGA-II are 801 points and 408 points, respectively. The optimal data

produced by the NSGA-G of the *S*, *D*, *f*, and *DT* were 370 rpm, 0.10 mm, 0.04 mm/rev, and 8 mm, respectively (Table 9). The optimal data produced by the NSGA-II of the *S*, *D*, *f*, and *DT* were 352 rpm, 0.10 mm, 0.04 mm/rev, and 7 mm, respectively. It can be stated that the NSGA-G provides a lower computational time, produces a higher number of feasible points, and better optimal results, as compared to the NSGA-II. Consequently, the *VH* is improved by 7.6 %, while the *Ra* is decreased by 40.7 % at the optimal solution, as compared to initial values.
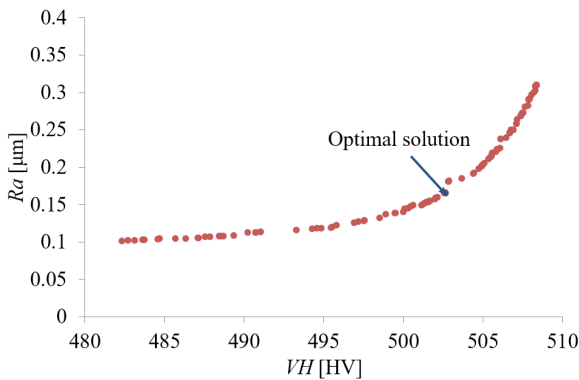

Fig. 12. *The Pareto front produced by the NSGA-G*

4.5 Scientific and Industrial Contributions

As a result, the average roughness and Vickers hardness of a new diamond burnishing process have been enhanced with the aid of optimum factors. The academic remarks are expressed as:

The proposed technique combining the ANN, CRITIC, and NSGA-G can be effectively utilized to find optimizing values of parameter inputs and responses for other diamond burnishing and machining processes.

The correlations developed by the BRFFNN approach can be applied to describe the complex data of the machining process.

The obtained data can be used in the practical diamond burnishing process to decrease the average roughness and enhance the Vickers hardness.

The industrial remarks are expressed as:
- A new diamond burnishing process comprising the MQL and double vortex tubes can be directly utilized in industrial applications for improving the surface properties of the external surface.
- The Pareto graphs can be applied to select optimal values of parameter inputs and responses for different burnishing aims.
- The CL efficiency of different machining operations (turning, milling, and grinding) can be enhanced with using the proposed system.
- The *Ra* and *VH* models developed BRFFNN approach can be precisely utilized to calculate the machining targets for different deployments.

4.6 Evaluation of the total diamond burnishing cost

The total diamond burnishing cost (*TDC*) is a summarization of the operation cost, lighting cost, depreciation cost, energy cost, tool cost, fluid cost, and cleaning cost. The *TDC* model is expressed as:

$$TDC = (C_o \times N_{db} \times \frac{t_{db}}{3600}) + (C_e \times P_{LT} \times \frac{t_{db}}{3600})$$
$$+ (\frac{C_{mi} - C_{sv}) \times t_{db}}{M_l \times 3600}) + (\frac{C_e \times P_{db} \times t_{db}}{3600 \times \eta})$$
$$+ (\frac{C_T \times t_{db}}{t_T}) + (F \times C_l \times 60 \times \frac{t_{db}}{3600})$$
$$+ (C_c \times F \times \frac{t_h}{3600}), \tag{15}$$

where C_o, N_{db}, and t_{db} are the unit operator cost, the number of operators, and machining time, respectively. C_e and P_L are the unit energy cost and lighting power, respectively. C_{mi}, C_{sv}, and t_{db} are the initial cost, salvage value, and useful life, respectively. C_e, P_{db}, and η present the unit energy cost, power used in the machining time, and the working efficiency of the machine tool, respectively. C_T and T_T are the unit cost

Table 9. *Optimization results generated by the BRNN-CRITI-NSGAG*

Method	Optimization parameters				Responses	
	S [rpm]	*D* [mm]	*f* [mm/rev]	*DT* [mm]	*Ra* [µm]	*VH* [HV]
Initial values	630	0.06	0.04	6	0.27	467.2
NSGA-G	630	0.10	0.05	8	0.16	502.6
NSGA-II	352	0.10	0.04	7	0.18	497.2
Improvement [%]					40.7	7.6

and useful life of the diamond tool tip, respectively. C_l, F, and C_c present the unit cost, flow rate of the fluid, and the unit cost of the cleaning operation, respectively. Table 10 presents the experimental coefficients for the TDC model. The *TDC* value is decreased by 20 % at the selected optimality, as compared to the common values (Table 11).

Table 10. *The experimental coefficients for estimating total diamond burnishing cost*

C_o [USD/h]	N_{db}	C_{mu} [USD]	C_{sv} [USD]	M_l [h]	C_e [USD/kWh]
8.2	1	61500	4000	20000	0.14

C_T [USD]	t_T [s]	F [ml/h]	C_l [USD/l]	C_c [USD/l]
13.8	3000	80	2	0.46

Table 11. *The reduction in the total diamond burnishing cost*

| Method | Optimization parameters | | | | Cost |
	S [rpm]	D [mm]	f [mm/rev]	DT [mm]	TDC [USD]
Common values	630	0.06	0.04	6	2.45
Optimal values	630	0.10	0.05	8	1.96
Reduction [%]					20.0

5 CONCLUSIONS

In this study, a new single diamond burnishing process was proposed and optimized to improve the Vickers hardness and decrease the average roughness. The parameter inputs were the S, D, f, and DT. The CRITIC method was applied to compute the weights, while the BRFFNN approach was utilized to develop the response model in terms of the optimizing factors. The obtained findings can be expressed as:

1. To enhance the Vickers hardness, the highest DT is applied, while the lowest values of the S, f, and DT are recommended. To decrease the average roughness, the highest values of the S, D, and DT are applied, while the lowest f is encouraged.
2. For the Ra, the f is named as the most effective parameter, followed by the S, D, and DT, respectively. For the VH, the S is named as the most effective parameter, followed by the f, D, and DT, respectively.
3. The optimal data of the S, D, f, and DT were 370 rpm, 0.10 mm, 0.04 mm/rev, and 8 mm, respectively. The VH was improved by 7.6 % while the Ra was decreased by 40.7 %. The total diamond burnishing cost could be decreased by 20 % at the optimal solution.

4. This investigation considered the average roughness and Vickers hardness of a new single diamond burnishing. Further work with more objectives, such as the wear rate, energy consumption, and grain size will be addressed.

6 REFERENCES

[1] Zaman, P.B., Dhar, N.R. (2020). Multi-objective optimization of double-jet MQL system parameters meant for enhancing the turning performance of Ti-6Al-4V Alloy. *Arabian Journal for Science and Engineering*, vol. 45, p. 9505-9526, **DOI:10.1007/s13369-020-04806-x.**

[2] Tamang, S.K., Chandrasekaran, M., Sahoo, A.K. (2018). Sustainable machining: an experimental investigation and optimization of machining Inconel 825 with dry and MQL approach. *Journal of the Brazilian Society of Mechanical Sciences and Engineering*, vol. 40, art. ID 374, **DOI:10.1007/s40430-018-1294-2.**

[3] Zan, Z., Guo, K., Sun, J., Wei, X., Tan, Y., Yang, B. (2021). Investigation of MQL parameters in milling of titanium alloy. *The International Journal of Advanced Manufacturing Technology*, vol. 116, p. 375-388, **DOI:10.1007/s00170-021-07441-4.**

[4] Sen, B., Mia, M., Mandal, U.K., Dutta, B., Mondal, S.P. (2019). Multi-objective optimization for MQL-assisted end milling operation: an intelligent hybrid strategy combining GEP and NTOPSIS. *Neural Computing & Applications*, vol. 31, p. 8693-8717, **DOI:10.1007/s00521-019-04450-z.**

[5] Van, A.L., Nguyen, T.T. (2022). Investigation and optimization of MQL system parameters in the roller-burnishing process of hardened steel. *Strojniški vestnik - Journal of Mechanical Engineering*, vol. 68, no. 3, p. 155-165, **DOI:10.5545/sv-jme.2021.7473.**

[6] Nguyen, T.T., Nguyen, T.A., Trinh, Q.H. Le, X.B., Pham, L.H., Le, X.H. (2022). Artificial neural network-based optimization of operating parameters for minimum quantity lubrication-assisted burnishing process in terms of surface characteristics. *Neural Computing & Applications*, vol. 34, p. 7005-7031, **DOI:10.1007/s00521-021-06834-6.**

[7] Sachin, B., Narendranath, S., Chakradhar, D (2019). Selection of optimal process parameters in sustainable diamond burnishing of 17-4 PH stainless steel. *Journal of the Brazilian Society of Mechanical Sciences and Engineering*, vol. 41, art. ID 219, **DOI:10.1007/s40430-019-1726-7.**

[8] Mahapatro, K., Krishna, P.V. (2022). Influence of flow parameters in the dual nozzle CO2-based vortex tube cooling system during turning of Ti-6Al-4V. *Proceedings of the Institution of Mechanical Engineers, Part C: Journal of Mechanical Engineering*, vol. 236, no. 9, **DOI:10.1177/09544062211057495.**

[9] Singh, R., Dureja, J.S., Dogra, M., Gupta, M.K., Jamil, M., Mia, M. (2020). Evaluating the sustainability pillars of energy and environment considering carbon emissions under machining ofTi-3Al-2.5V. *Sustainable Energy Technologies and Assessments*, vol. 42, art. ID 100806, **DOI:10.1016/j.seta.2020.100806.**

[10] Gupta, M.K., Mia, M., Singh, G., Pimenov, D.Y., Sarikaya, M., Sharma, V.S. (2019). Hybrid cooling-lubrication strategies to improve surface topography and tool wear in sustainable turning of Al 7075-T6 alloy. *The International Journal of Advanced Manufacturing Technology*, vol. 101, p. 55-69, **DOI:10.1007/s00170-018-2870-4**.

[11] Mia, M., Singh, G., Gupta, M.K., Sharma, V.S. (2018). Influence of Ranque-Hilsch vortex tube and nitrogen gas assisted MQL in precision turning of Al 6061-T6. *Precision Engineering*, vol. 53, p. 289-299, **DOI:10.1016/j.precisioneng.2018.04.011**.

[12] Duc, T.M., Long, T.T., Van Thanh, D. (2020). Evaluation of minimum quantity lubrication and minimum quantity cooling lubrication performance in hard drilling of Hardox 500 steel using Al2O3 nanofluid. *Advances in Mechanical Engineering*, vol 12, no. 2, p. 1-12, **DOI:10.1177/1687814019888404**.

[13] Sharma, A., Singh, R.C., Singari, R.M. (2020). Optimization of machining parameters during cryogenic turning of AISI D3 steel. *Sādhanā*, vol. 45, art. ID 124, **DOI:10.1007/s12046-020-01368-4**.

[14] Khan, M.A., Jaffery, S.H.I., Khan, M., Younas, M., Butt, S.I., Warsi, S.S. (2020). Multi-objective optimization of turning titanium-based alloy Ti-6Al-4V under dry, wet, and cryogenic conditions using gray relational analysis (GRA). *The International Journal of Advanced Manufacturing Technology*, vol. 106, p. 3897-3911, **DOI:10.1007/s00170-019-04913-6**.

[15] Mia, M., Khan, M.A., Dhar, N.R. (2017). Study of surface roughness and cutting forces using ANN, RSM, and ANOVA in turning of Ti-6Al-4V under cryogenic jets applied at flank and rake faces of coated WC tool. *The International Journal of Advanced Manufacturing Technology*, vol. 93, p. 975-991. **DOI:10.1007/s00170-017-0566-9**.

[16] Sachin, B., Narendranath, S., Chakradhar, D. (2018). Experimental evaluation of diamond burnishing for sustainable manufacturing. *Materials Research Express*, vol. 5, no. 10, art. ID 106514, **DOI:10.1088/2053-1591/aadb0a**.

[17] Sachin, B., Narendranath, S., Chakradhar, D. (2020). Application of desirability approach to optimize the control factors in cryogenic diamond burnishing. *Arabian Journal for Science and Engineering*, vol. 45, p. 1305-1317, **DOI:10.1007/s13369-019-04326-3**.

[18] Maximov, J.T., Duncheva, G.V., Anchev, A.P., Dunchev, V.P. (2020). Smoothing, deep, or mixed diamond burnishing of low-alloy steel components - optimization procedures. *The International Journal of Advanced Manufacturing Technology,* vol. 106, p. 1917-1929, **DOI:10.1007/s00170-019-04747-2**.

[19] Maximov, J.T., Duncheva, G.V., Anchev, A.P., Dunchev, V.P., Ichkova, M.D. (2020). Improvement in fatigue strength of 41Cr4 steel through slide diamond burnishing. *Journal of the Brazilian Society of Mechanical Sciences and Engineering*, vol. 42, art. ID 197, **DOI:10.1007/s40430-020-02276-8**.

[20] Duncheva, G.V., Maximov, J.T., Anchev, A.P., Dunchev, V.P., Agirov, Y.B. (2022). Multi-objective optimization of the internal diamond burnishing process. *Materials and Manufacturing Processes*, vol. 37, no. 4, p. 428-436, **DOI:10.1080/10426914.2021.1981937**.

[21] Milčić, D., Alsammarraie, A., Madić, M., Krstić, V., Milčić, M. (2021). Predictions of friction coefficient in hydrodynamic journal bearing using artificial neural networks. *Strojniški vestnik - Journal of Mechanical Engineering*, vol. 67, no. 9, p. 411-420, **DOI:10.5545/sv-jme.2021.7230**.

[22] Sivakumar, A., Bagath Singh, N., Sathiamurthi, P. Karthi Vinith, K.S. 3 (2021). Extremal-micro genetic algorithm model for time-cost optimization with optimal labour productivity. *Strojniški vestnik - Journal of Mechanical Engineering*, vol. 67, no. 12, p. 682-691, **DOI:10.5545/sv-jme.2021.7406**.